Sigurlaug Hjaltadóttir
Kristín S. Vogfjörð
Þóra Árnadóttir
Páll Einarsson
Peter Suhadolc

A model of the release of the two June 2000 earthquakes based on all available observations

A Model of the Release of the Two June 2000 Earthquakes Based on All Available Observations

Sigurlaug Hjaltadóttir, Kristín S. Vogfjörð, Þóra Árnadóttir, Páll Einarsson and Peter Suhadolc

Introduction
Detailed slip models for the June 17 and June 21 main shocks have been estimated from a joint inversion of InSAR and GPS data (Pedersen et al., 2003) and strong motion data (Suhadolc and Sandron, 2005). The sub-surface fault structures of the two events have also been mapped by relative relocations of aftershocks (Hjaltadóttir and Vogfjörð, 2005) and the surface fractures in the two epicentral areas have been mapped (Clifton and Einarsson, 2005). The following is a summary of the main results from the PREPARED 4-work packages and a comparison of the models.

June 17 fault:

Mapping of aftershocks
The June 17th fault is roughly 12.5 km long and 10 km deep. Aftershocks on the fault are mainly confined to the fault margins, mostly below 3 km, and a cluster in the center of the fault, around the hypocenter (Figure 1). During the first 24 hours however, aftershocks were distributed over the entire fault.

The J17 fault is near vertical, the overall strike is ~7°, but it is composed of many smaller sections with differing strikes. Above 8 km depth the aftershocks display a rather discontinuous pattern composed of three main patches, each approximately 2-3.5 km long (Figure 2). The central patch is very planar and was active throughout the year. Its strike (~11 degrees) is slightly east of the overall strike of the fault. Activity on the northernmost fault section is mostly near its northern edge, where it branches into a few short N-striking planes. The southernmost section is more continuous and bends westwards with decreasing latitude. At the southern tip the fault jumps half a kilometer to the west and continues on a ~2 km-long-segment. West of the southern edge, a few small faults were also activated. Their strikes are generally west of north.

Below 8 km depth the aftershocks define a continuous fault trace, but with kinks at the intersections of the main sections above. Below the northernmost fault section, the bottom appears to be composed of a few smaller en-echelon faults and then breaks up into separate parallel branches farther north. Activity on the southernmost fault patch, on the other hand, appears to be continuous and more linear, bending slightly westward towards the southern end.

Inversion of strong motion data
Strong motion data is inverted for distribution of seismic moment on the fault, with total moment constrained by the observed teleseismic moment. Strike of the fault was assumed 4° and dip 87°. The results, calculated on a grid with 2 km resolution, show that most of the moment is released on the central patch, with a peak below the hypocenter, extending ~8 km northwards along the fault and down to ~8 km depth near the center. A second maximum is located at shallow depth (3 km) roughly 6 km south of the hypocenter. Two additional peaks in momentum are also obtained near the surface (1 km depth), one at the northern margin of the fault and the other above the hypocenter. In Figure 1 seismic moment is converted to displacement using a constant shear

modulus. If account is taken of the increase in velocity with depth (increasing shear modulus with depth), displacement at the surface increases significantly, which is questionable.
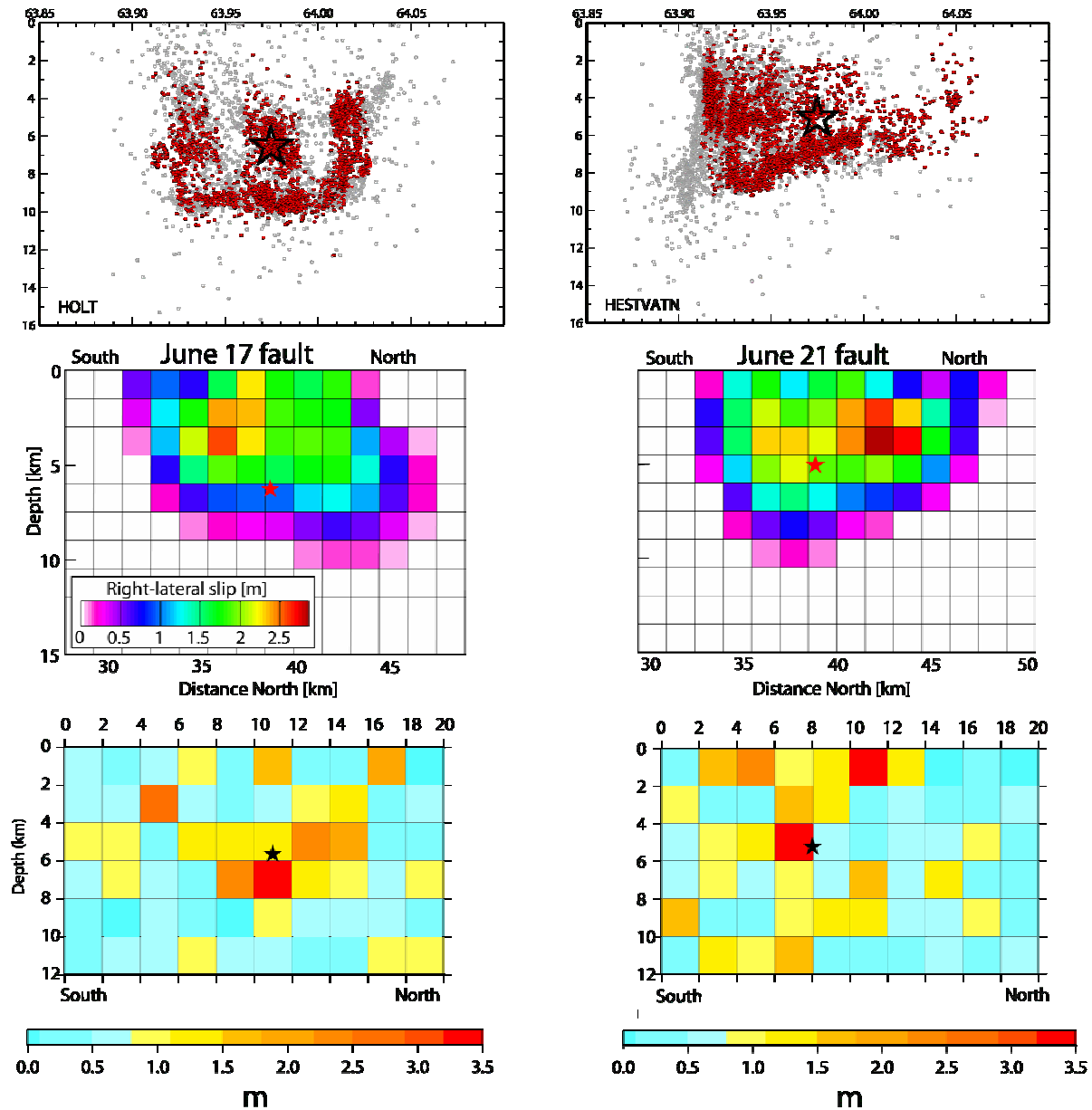

Figure 1. *Left: The June 17 fault. Right: The June 21 fault.*
Top: Relatively located aftershock distribution on the fault planes in vertical view from east, with coloured events from Figure 2 shown in red. Middle: Right-lateral fault slip models for the June 17 and June 21 main shocks derived from joint inversion of InSAR and GPS data. The size of each grid cell is 1.5X1.5 km. Bottom: Slip distribution obtained from strong motion data. The value for each grid cell is plotted in a discrete coloured scale of intensities. The size of each grid cell is 2X2 km. The stars show the main shock hypocenter locations.

4

Inversion of geodetic data
Inversion of GPS and InSAR data for slip on the fault, in 1.5 km cells, shows the displacement approximately covers the aftershock region, but slip is greatest above and south of the hypocenter. Maximum slip is attained between 3 and 4 km depth, roughly 2 km south of the hypocenter, which is both shallower and south of the maximum obtained from the strong motion inversion.

Mapping of surface rupture
Mapped surface rupture shows a discontinuous pattern distributed asymmetrically along the fault defined by the relocated event distribution. Most surface ruptures occur along NNE-striking left-stepping en-echelon segments within a 2 km wide zone, approximately centered on the fault, though the majority occurs on the western edge (Figure 2). When compared to the geodetic and strong motion results, the distribution and intensity of surface rupture agrees well with the geodetic maximum slip, south of the hypocenter, and with the maximum moment, just below the hypocenter. There, a 2.5 km long continuous fracture was observed, west of the event distribution on the center fault patch. Another 3-km-long segment extends northwards approximately 1 km west of the fault, but the northernmost segments lie approximately parallel above and just east of the event distribution, which also shows fracture on parallel segments at depth. To the south, the surface ruptures fall just east of and along the southernmost fault patch.

June 21 fault:

Mapping of aftershocks
During the time period between the two main shocks (June 17th-21st), seismic activity in the epicentral area of the June 21st fault was mainly along the bottom of the eventual fault and along the trace of the mapped conjugate surface faults at ~63.95°, extending westward from the main fault. During the first 24 hours following the June 21st event, the aftershocks however were distributed over the entire main fault up to about 1 km depth. After that, activity concentrated along the bottom, except at the southern end, where it was distributed over the whole depth range and continued throughout the year.

South of the hypocenter, aftershocks are evenly distributed over the fault, while north of the hypocenter the activity is sparser and mostly concentrated near the bottom. The overall fault length, defined by the aftershocks, is 16.5 km and its strike is 179°. The fault depth increases southward, from ~7 km on the northern half to ~10 km at the southern margin (see Figure 1).

Near the hypocenter the fault branches into two faults with different dips. The southern half is vertical and extends north to latitude 64°, terminating at the southern shore of lake Hestvatn. The northern half dips 77° east and extends from the hypocenter to the northern margin of the fault (64.05° N). Both branches continue with a similar northerly strike and follow approximately the same trace at the bottom, creating an approximately 3 km long wedge north of the hypocenter. The intersection of the dipping segment with the surface, approximately matches the mapped surface ruptures west of lake Hestvatn. At the southern terminus, the fault is broken up into many small fault segments of 1-2 km diameter and with varying strike.

Near the location of the mapped conjugate surface-rupture (see Figure 2), the earthquake distribution is denser and extends westward, mostly on short easterly striking segments. About 3

km farther south, a second set of conjugate faults, extending over a wide depth range (2-9 km) is also defined by the seismicity.
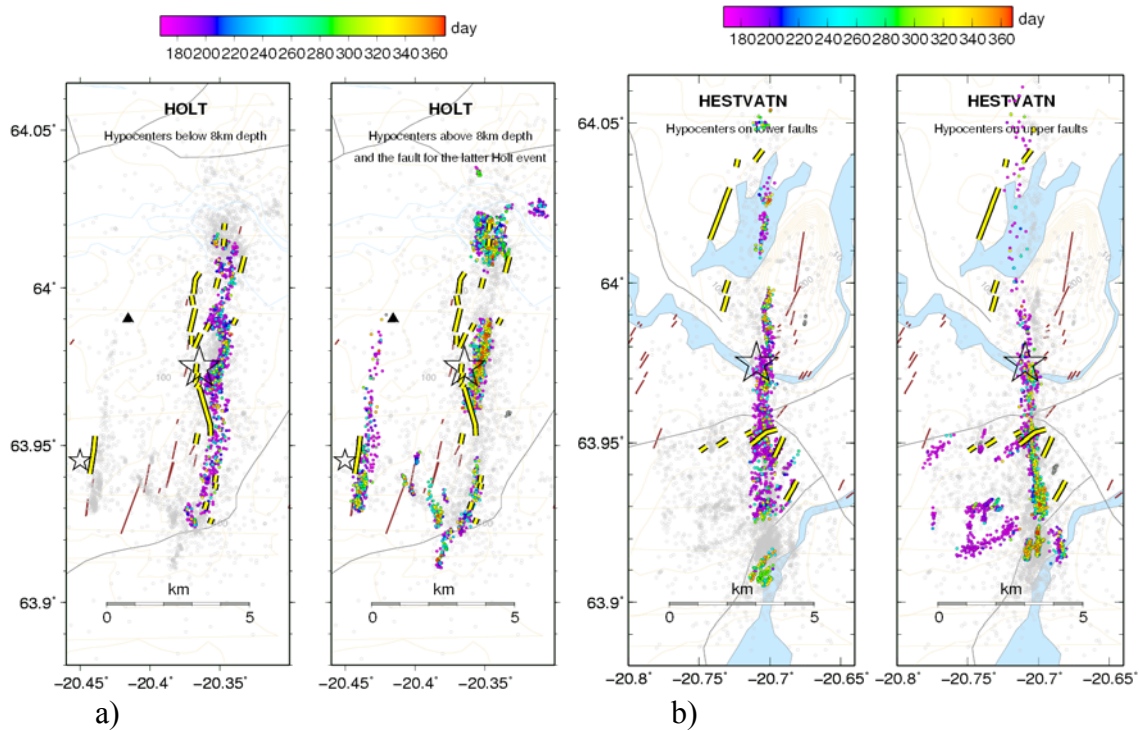

Figure 2. *The aftershocks and surface ruptures on the Holt and Hestvatn faults. The hypocentre of the two M=6.5 events are denoted with stars. The hypocenter for the second Holt event, occuring roughly 2 minutes later, is also marked on the left map by a smaller star. All events are shown in the background in grey. Events on identified faults are displayed in colour, according to age (from June 17th to December 31st, and June 21st to December 31st, respectively) and for different depth ranges. Yellow lines display surface rupture from 2000. Note that the roads on the map (thin black lines) are shifted ~ 0.7km north-westwards from their actual location.*

Inversion of strong motion data

Inversion of strong motion data for moment distribution on the fault shows that the maximum in moment release is located at a depth of 5 km, ~1 km south of the hypocenter, which is also at the intersection with the westward extending conjugate fault (where surface rupture was observed). An increase in moment release follows approximately the distribution of aftershocks along the bottom of the fault, increasing in depth from 7 km on the northern half of the fault to 11 km just south of the hypocenter. Two additional maxima are located just below the surface. The smaller one is 3 km south of the hypocenter, the other is 3 km north of the hypocenter, approximately at the end of the vertical section of the fault.

Strike of the fault was assumed 358° and dip 90°, according to those defined by the aftershock distribution, except for the northern half of the fault, where the aftershocks show the fault branching out and changing dip.

Table 1. *Fault parameters for the June 2000 earthquakes estimated from different datasets. Latitude and longitude is for the center of the fault plane at the upper edge, except for the best double couple solutions, for which latitude, longitude and depth denote the location of the hypocenter of the main shock on each fault. Modified from Pedersen et al. (2003).*

June 17	Origin time	Length	Width	Depth	Lat	Lon	Strike	Dip	Rake	Strike slip	Dip slip	M_0	M_w
		(km)	(km)	(km)	(°)	(°)	(N°E)	(°E)	(°)	(m)	(m)	(Nm) x10^{18}	
Uniform slip	-	10.6	7.9	0.0*	63.973	-20.347	1	87*	180	1.7	0	4.4	6.4
Distributed slip	-	~15	~10	0.0	63.973	-20.347	2*	87*	180	0.0-2.6	0*	4.5	6.4
Árnadóttir et al. (2001)	-	9.5	9.8	0.1	63.970	-20.351	3	90*	174	2.0	0.2	5.6	6.5
Pedersen et al. (2001)	-	16.0	10.0*	0.0*	63.979	-20.342	5*	86*	175	0.3-2.4	0.0-0.2	5.4	6.5
IMO **	-	12.5	10	-	63.975	-20.35	7	89	-	-	-	-	-
IMO ***	15:40:40.987	-	-	6.54	63.975	-20.365	19	76	-154	-	-	2.7	6.3
NEIC	-	-	-	-	63.966	-20.487	-1	75	173	-	-	4.3	6.4
Harvard CMT	-	-	-	-	63.99	-20.47	4	87	-164	-	-	7.1	6.5

June 21	Origin time	Length	Width	Depth	Lat	Lon	Strike	Dip	Rake	Strike slip	Dip slip	M_0	M_w
	hh:mm:ss	(km)	(km)	(km)	(°)	(°)	(N°E)	(°E)	(°)	(m)	(m)	(Nm)x10^{18}	
Uniform slip	-	11.9	8.2	0.0*	63.987	-20.705	0	90*	180	1.8	0	5.3	6.4
Distributed slip	-	~15	~10	0.0	63.987	-20.705	0*	90*	180	0.0-2.9	0*	5.0	6.5
Árnadóttir et al. (2001)	-	12.3	8.0	0.0*	63.984	-20.691	0.5	90*	180	1.5	0	4.5	6.4
Pedersen et al. (2001)	-	15.0	9.0*	0.0*	63.982	-20.703	0*	90*	180	0.5-2.2	0	5.1	6.4
IMO **	-	16.5	7-10	-	63.798	20.705	179	89[1]	-	-	-	-	6.5
IMO ***	00:51:46.971	-	-	5.08	63.975	-20.709	166	50	160	-	-	10.3	6.7
NEIC	-	-	-	-	63.980	-20.758	-4	79	-173	-	-	5.0	6.4
Harvard CMT	-	-	-	-	63.98	-20.85	2	85	-167	-	-	5.4	6.5

* Parameters held fixed in the modeling.
** IMO's results from relative location of aftershocks. [1]Dip north of hypocenter changes to 77°, as discussed in the text.
*** IMO's best double couple solutions for the main shocks; origin time, latitude, longitude and depth have been improved by double-difference relative relocation method.
NEIC see U.S.G.S; Harvard CMT see Dziewonski et al., 2001.

Inversion of geodetic data

Inversion of GPS and InSAR data for slip on the fault shows the displacement approximately covers the aftershock region. The maximum depth of 10 km is attained in the south center of the fault. Maximum slip is obtained above the hypocenter, at approximately 4 km depth, 3-4 km north of the hypocenter. This does not agree with the strong motion results. However, the dipping northern fault segment defined by the aftershocks, could account for the apparent increased slip north of the hypocenter, since the geodetic solution allows only constant dip on the whole fault. The smaller peak in slip, obtained at the same depth and 1-3 km south of the hypocenter agrees rather well with the strong motion results.

The geodetic data record the co-seismic deformation as well as any rapid transient motion that occurred during the data acquisition (~2 weeks for the GPS, ~1 month for the InSAR). This may

explain some differences in the distributed slip models obtained from the geodetic and strong motion data.

Mapping of surface rupture
Mapped surface rupture shows a discontinuous pattern distributed asymmetrically along the fault defined by the relocated event distribution. The pattern is more complex than for the June 17 fault. At the southern end of the fault, where the clustering of aftershocks is the densest, no surface rupture has been observed, but 2-3 km farther north, a NNE trending segment lies west of the fault, almost in continuation of the largest left lateral conjugate fault, mapped at depth (Figure 2b). Another NNE trending segment of similar length is observed, where the large conjugate fault extends from the fault to the west, 2.5-3 km south of the hypocenter. It is 2.5 km long and is by far the longest E-W trending segment observed in the SISZ and shows a left lateral strike slip motion. This segment is not clearly seen by the relocated event distribution, but there is an indication of a fault, extending ~1 km to the SW from the main fault. The results from the strong motion data show a small maximum just below the surface at the location of the conjugate fault. No surface rupture has been observed above the epicenter, but 1.5-2 km further north, segments are mapped well west of the linear event distribution, approximately where the 77°-dipping fault intersects the surface.

Acknowledgements

Figures 1 (top) and 2 were made by using the GMT public domain software (Wessel and Smith, 1998).

References

Árnadóttir, T., S. Hreinsdóttir, G. Gudmundsson, P. Einarsson, M. Heinert, C. Völkssen, 2001. Crustal deformation measured by GPS in the South Iceland Seismic Zone due to two large earthquake in June 2000, *Geophys. Res. Lett*. 28, 4031-4034.

Clifton, Amy, Páll Einarsson, 2005. Styles of Surface rupture accompanying the June 17 and 21, 2000 earthquakes in the South Iceland Seismic Zone. *Tectonophysics*, 396, pp. 141-159.

Dziewonski, A. M., G. Ekstrom, N. N. Maternovskaya, 2001. Centroid-moment tensor solutions for April-June 2000, *Phys. Earth Planet. Inter*. 123, 1-14.

Hjaltadóttir, Sigurlaug and Kristín S. Vogfjörð, 2005. Subsurface fault mapping in South-West Iceland by relative location of aftershocks of the June 2000 earthquakes. *Rit Veðurstofu Íslands,* 21, VÍ-ES01.

Pedersen, R., F. Sigmundsson, K. L. Feigl, T. Árnadóttir, 2001. Co-seismic interferograms of two Ms=6.6 earthquakes in the South Iceland Seismic Zone, June 2000, *Geophys. Res. Lett*. 28, 3341-3344.

Pedersen, R., S. Jónsson, Th. Árnadóttir, F. Sigmundsson, and K. L. Feigl, 2003. Fault slip distribution of two Mw=6.5 earthquakes in South Iceland estimated from joint inversion of InSAR and GPS measurements, *Earth and Planetary Science Letters*, 213, 487-502.

Suhadolc, P and D. Sandron, 2005. WP 4.2 Fault slip distribution of the two June 2000 Mw 6.5 earthquake in South Iceland estimated by strong motion inversion. In R. Stefánsson, editor, PREPARED, third periodic report, 2005. *Icelandic Meteorological Office, report* in press.

U.S.G.S., National Earthquake Information Center: Previous Fast Moments, http://wwwneic.cr.usgs.gov/neis/FM/previous/0006.html

Wessel, P. and W.H.F. Smith, 1998. New, improved version of Generic Mapping Tools Released. *Eos, Trans. AGU* 79, 579.